NASA TECHNICAL NOTE

NASA TN D-7712

MONTE CARLO ANALYSIS OF INACCURACIES IN ESTIMATED AIRCRAFT PARAMETERS CAUSED BY UNMODELED FLIGHT INSTRUMENTATION ERRORS

by Ward F. Hodge and Wayne H. Bryant

Langley Research Center

Hampton, Va. 23665

NATIONAL AERONAUTICS AND SPACE ADMINISTRATION • WASHINGTON, D. C. • FEBRUARY 1975

1. Report No. NASA TN D-7712	2. Government Accession No.	3. Recipient's Catalog No.
4. Title and Subtitle MONTE CARLO ANALYSIS OF INACCURACIES IN ESTIMATED AIRCRAFT PARAMETERS CAUSED BY UNMODELED FLIGHT INSTRUMENTATION ERRORS		5. Report Date February 1975
		6. Performing Organization Code
7. Author(s) Ward F. Hodge and Wayne H. Bryant		8. Performing Organization Report No. L-9411
9. Performing Organization Name and Address NASA Langley Research Center Hampton, Va. 23665		10. Work Unit No. 501-23-11-05
		11. Contract or Grant No.
12. Sponsoring Agency Name and Address National Aeronautics and Space Administration Washington, D.C. 20546		13. Type of Report and Period Covered Technical Note
		14. Sponsoring Agency Code

15. Supplementary Notes

16. Abstract

   An output error estimation algorithm was used to evaluate the effects of both static and dynamic instrumentation errors on the estimation of aircraft stability and control parameters. A Monte Carlo error analysis, using simulated cruise flight data, was performed for a high-performance military aircraft, a large commercial transport, and a small general aviation aircraft. The results indicate that unmodeled instrumentation errors can cause inaccuracies in the estimated parameters which are comparable to their nominal values. However, the corresponding perturbations to the estimated output response trajectories and characteristic equation pole locations appear to be relatively small. Control input errors and dynamic lags were found to be the most significant of the error sources evaluated.

17. Key Words (Suggested by Author(s)) Stability and control derivatives Parameter estimation Error analysis Instrumentation errors	18. Distribution Statement Unclassified — Unlimited STAR Category 02		
19. Security Classif. (of this report) Unclassified	20. Security Classif. (of this page) Unclassified	21. No. of Pages 34	22. Price* $3.75

MONTE CARLO ANALYSIS OF INACCURACIES IN ESTIMATED
AIRCRAFT PARAMETERS CAUSED BY UNMODELED
FLIGHT INSTRUMENTATION ERRORS

By Ward F. Hodge and Wayne H. Bryant
Langley Research Center

SUMMARY

An output error estimation algorithm was used to evaluate the effects of both static and dynamic instrumentation errors on the estimation of aircraft stability and control parameters. A Monte Carlo analysis, using simulated cruise flight data, was performed for a high-performance military aircraft, a large commercial transport, and a small general aviation aircraft. The effects of variations in the information content of the flight data, resulting from two different choices of control input maneuvers, were also determined.

The results indicate that unmodeled instrumentation errors can cause inaccuracies in the estimated parameters which are comparable to their nominal values. However, the corresponding perturbations to the estimated output response trajectories and characteristic equation pole locations appear to be relatively small. The magnitudes of these perturbations, for both longitudinal and lateral response modes, can vary appreciably with different classes of aircraft and with the information content of the flight data used. The most significant of the instrumentation errors evaluated were found to be the white noise and lag in the elevator position, the bias and lag in the aileron position, and the lags in the pitch and roll acceleration measurements. The perturbations they produce are much larger than those arising from the combined effects of static errors and white noise in the output response measurements.

INTRODUCTION

One of the important tasks associated with current efforts to improve the accuracy of estimating stability and control derivatives from flight data is to evaluate the effects of unmodeled errors in the measurements. Largely because less stringent accuracy requirements and marginal computational facilities formerly existed, suitable error-analysis algorithms for this purpose have appeared only recently. Two such algorithms, based on the minimization of output response errors, are described in reference 1. The

first approach furnishes statistics of the resulting parameter inaccuracies through the use of sensitivity coefficients in an ensemble technique, and the second provides this information by means of a Monte Carlo analysis of simulated flight data.

Reference 1 also reports an initial application of the ensemble algorithm where the effects of static errors (such as biases, scale factors, misalinements, center of gravity uncertainty, and vane corrections) were analyzed, assuming typical instrumentation and cruise flight conditions. The results, together with those presented in reference 2, indicated that these error sources can cause much larger parameter inaccuracies than those attributed to white noise in the output response measurements alone.

The results contained in reference 3 and this report extend the overall investigation in several respects. A principal objective of these studies was to evaluate the effects of additional error sources such as those arising from instrumentation dynamics and measurements of control inputs. The simulated data algorithm was used for this purpose, since these errors cannot be handled by the ensemble algorithm without introducing approximations which have not yet been evaluated. As stability and control derivatives are often estimated from flight data obtained for other purposes that may not require full excitation of the aircraft response modes, results were generated to examine the effects of varying the information content of the measurements. Similar data were obtained to determine further how much the results change with different classes of aircraft. In order to provide a more complete evaluation, the effects of parameter inaccuracies (caused by unmodeled instrumentation errors) on the output response trajectories and characteristic equation pole locations were also determined. Lastly, a sensitivity analysis was performed to identify the dominant error sources.

SYMBOLS

B	measurements bias vector
F,G	aircraft dynamics system matrices (eq. (4))
g	acceleration due to gravity, m/s^2
H,D	response measurements system matrices (eq. (3))
J	estimation algorithm performance function (eq. (1))
M	number of Monte Carlo runs

N   number of data samples

n   number of rows or columns

n_x, n_y, n_z body-axis components of aircraft linear acceleration, g units

O   null vector or matrix (eqs. (4) and (10))

P   parameter vector

p,q,r   roll, pitch, and yaw rates about body axes, respectively, rad/s or deg/s

$\dot{p}, \dot{q}, \dot{r}$ roll, pitch, and yaw acceleration about body axes, respectively, rad/s^2 or deg/s^2

R   covariance matrix of white measurement noise (eq. (17))

s   characteristic equation root (eq. (23))

T   matrix of scale factor, crosscoupling, and misalinement errors

t   time, s

U   control input vector

u,w   body-axis components of aircraft linear velocity, m/s

V   unperturbed nominal airspeed, m/s (table II)

W   white measurement noise vector

X   aircraft state vector

Y   output response vector

α angle of attack, rad or deg

β angle of sideslip, rad or deg

Γ	diagonal matrix of instrumentation time constants (eqs. (15) and (19))
$\delta_e, \delta_a, \delta_r$	elevator, aileron, and rudder deflections, respectively, deg
ϵ, γ	elements of T matrices (eqs. (12), (13), (14), and (17))
ζ	damping factor
σ	standard deviation
τ	time constant, s (table I)
ϕ, θ	roll and pitch attitude angles about body axes, respectively, rad or deg
ω	natural frequency

Subscripts:

ax,ay,az	body-axis components of accelerometer position relative to center of gravity
c	control input
D	Dutch roll
f	final value
I	indicated value
i,j,k	discrete time sample indices, or matrix or vector elements
L	lagged value
m	measured value
nx,ny,nz	linear accelerometers
o	initial or unperturbed value
r	roll subsidence

4

s   spiral divergence

sp   short period

vx   vane location along X-axis

xcg,ycg,zcg   components of center of gravity location

y   output response

Notations:

E( )   statistical expectation

$(\ )^{-1}$ matrix inversion

$(\ )^{T}$ matrix transposition

$(\hat{\ })$ estimated value

$\Delta(\ )$ increment or perturbation value

$(\bar{\ })$ mean value

$(\dot{\ })$ time derivative

METHOD OF ANALYSIS

The Monte Carlo error analysis employed in the study is described in three steps which, respectively, outline the formulation of the simulated data algorithm, the modeling of the various instrumentation errors, and the pertinent statistical computations.

Simulated Data Algorithm

The essential feature of the simulated data concept is that the parameter inaccuracies caused by unmodeled instrumentation errors are obtained simply as the differences between the assumed true values of the parameters and those estimated from simulated flight data which contain the unmodeled errors. The estimation algorithm used for this purpose is that of reference 4, which minimizes the output response error in the least squares sense by using a performance function of the form

$$J(P) = \int_{t_o}^{t_f} \left[Y_m(t) - \hat{Y}(P,t) \right]^T R^{-1} \left[Y_m(t) - \hat{Y}(P,t) \right] dt$$

where $Y_m(t)$ and $\hat{Y}(P,t)$ are, respectively, the measured and estimated output response vectors over a data-gathering period $\left[t_o, t_f \right]$, and R^{-1} is a weighting matrix defined later in equation (17). Since the algorithm is implemented in discrete form for computational reasons, $J(P)$ is approximated

$$J(P) \approx \sum_{i=1}^{N} \left[Y_{mi} - \hat{Y}(P)_i \right]^T R^{-1} \left[Y_{mi} - \hat{Y}(P)_i \right] \tag{1}$$

which represents N samples of the output error during $\left[t_o, t_f \right]$. The corresponding least squares normal equations $\partial J/\partial P = 0$ are then solved for $\hat{P}$ by means of the differential correction procedure

$$\hat{P}_{j+1} = \hat{P}_j + \Delta\hat{P}_j$$

$$= \hat{P}_j + \left[\sum_{i=1}^{N} \left(\frac{\partial \hat{Y}_i}{\partial P} \right)^T R^{-1} \left(\frac{\partial \hat{Y}_i}{\partial P} \right) \right]^{-1} \left[\sum_{i=1}^{N} \left(\frac{\partial \hat{Y}_i}{\partial P} \right)^T R^{-1} \left(Y_{mi} - \hat{Y}_i \right) \right] \tag{2}$$

which is also called a quasilinearization or modified Newton-Raphson minimization technique. (See ref. 4.) The convergence criteria used for the present study was $\left| \Delta\hat{P}_j \right| \leq \left| 0.01\hat{P}_j \right|$ simultaneously for each parameter.

The estimated output $\hat{Y}_i$ required in evaluating equation (2) is modeled as

$$\hat{Y}_i = H(P)\hat{X}_i + D(P)U_{mi} \tag{3}$$

where the state vector $\hat{X}_i$ is obtained by numerical integration of the aircraft dynamical equations

$$\frac{d}{dt}\left(\hat{X}_i \right) = F(P)\hat{X}_i + G(P)U_{mi} \qquad \left(\hat{X}_0 = 0 \right) \tag{4}$$

The particular forms of these equations used for the three aircraft response modes are defined as follows: For the longitudinal motions, the forms of equations (3) and (4) are given, respectively, as

$$
\begin{bmatrix} \Delta\theta \\ \Delta q \\ \Delta\alpha \\ \Delta u \\ \Delta n_x \\ \Delta n_z \\ \Delta\dot{q} \end{bmatrix} = \begin{bmatrix} 1 & 0 & 0 & 0 \\ 0 & 1 & 0 & 0 \\ 0 & 0 & \dfrac{\cos\alpha_o}{V} & \dfrac{-\sin\alpha_o}{V} \\ 0 & 0 & 0 & 1 \\ 0 & 0 & \dfrac{X_w}{g} & \dfrac{X_u}{g} \\ 0 & 0 & \dfrac{Z_w}{g} & \dfrac{Z_u}{g} \\ 0 & M_q & M_w & M_u \end{bmatrix} \begin{bmatrix} \Delta\theta \\ \Delta\dot{q} \\ \Delta w \\ \Delta u \end{bmatrix} + \begin{bmatrix} 0 \\ 0 \\ 0 \\ 0 \\ 0 \\ \dfrac{Z_{\delta e}}{g} \\ M_{\delta e} \end{bmatrix} \begin{bmatrix} \Delta\delta e \end{bmatrix} \tag{5}
$$

and

$$
\begin{bmatrix} \Delta\dot{\theta} \\ \Delta\dot{q} \\ \Delta\dot{w} \\ \Delta\dot{u} \end{bmatrix} = \begin{bmatrix} 0 & 1 & 0 & 0 \\ 0 & M_q & M_w & M_u \\ -g\sin\theta_o & V\cos\alpha_o & Z_w & Z_u \\ -g\cos\theta_o & -V\sin\alpha_o & X_w & X_u \end{bmatrix} \begin{bmatrix} \Delta\theta \\ \Delta q \\ \Delta w \\ \Delta u \end{bmatrix} + \begin{bmatrix} 0 \\ M_{\delta e} \\ Z_{\delta e} \\ 0 \end{bmatrix} \begin{bmatrix} \Delta\delta e \end{bmatrix} \tag{6}
$$

where the parameter vector P to be estimated is

$$
P = \begin{bmatrix} M_q M_w Z_w M_{\delta e} Z_{\delta e} & \vdots & M_u Z_u X_u X_w \end{bmatrix}^T
$$

and the short period approximations of equations (5) and (6) are obtained by deleting Δu and Δn_x along with all their factors and the last four elements of the P vector. The corresponding expressions for the lateral-directional motions are given by

$$
\begin{bmatrix} \Delta\beta \\ \Delta p \\ \Delta r \\ \Delta\phi \\ \Delta n_y \\ \Delta\dot{p} \\ \Delta\dot{r} \end{bmatrix}
=
\begin{bmatrix}
1 & 0 & 0 & 0 \\
0 & 1 & 0 & 0 \\
0 & 0 & 1 & 0 \\
0 & 0 & 0 & 1 \\
\dfrac{V}{g}Y_\beta & 0 & 0 & 0 \\
L_\beta^* & L_p^* & L_r^* & 0 \\
N_\beta^* & N_p^* & N_r^* & 0
\end{bmatrix}
\begin{bmatrix} \Delta\beta \\ \Delta p \\ \Delta r \\ \Delta\phi \end{bmatrix}
+
\begin{bmatrix}
0 & 0 \\
0 & 0 \\
0 & 0 \\
0 & 0 \\
\dfrac{Y_{\delta a}}{g} & \dfrac{Y_{\delta r}}{g} \\
L_{\delta a}^* & L_{\delta r}^* \\
N_{\delta a}^* & N_{\delta r}^*
\end{bmatrix}
\begin{bmatrix} \Delta\delta a \\ \Delta\delta r \end{bmatrix}
\tag{7}
$$

and

$$
\begin{bmatrix} \Delta\dot{\beta} \\ \Delta\dot{p} \\ \Delta\dot{r} \\ \Delta\dot{\phi} \end{bmatrix}
=
\begin{bmatrix}
Y_\beta & \sin\alpha_o & -\cos\alpha_o & \dfrac{g}{V}\cos\theta_o \\
L_\beta^* & L_p^* & L_r^* & 0 \\
N_\beta^* & N_p^* & N_r^* & 0 \\
0 & 1 & \tan\theta_o & 0
\end{bmatrix}
\begin{bmatrix} \Delta\beta \\ \Delta p \\ \Delta r \\ \Delta\phi \end{bmatrix}
+
\begin{bmatrix}
Y_{\delta a} & Y_{\delta r} \\
L_{\delta a}^* & L_{\delta r}^* \\
N_{\delta a}^* & N_{\delta r}^* \\
0 & 0
\end{bmatrix}
\begin{bmatrix} \Delta\delta a \\ \Delta\delta r \end{bmatrix}
\tag{8}
$$

where

$$
P = \begin{bmatrix} Y_\beta L_\beta^* N_\beta^* L_p^* N_p^* L_r^* N_r^* Y_{\delta a} L_{\delta a}^* N_{\delta a}^* Y_{\delta r} L_{\delta r}^* N_{\delta r}^* \end{bmatrix}^T
$$

and is modified with respect to the derivatives bearing an asterisk to account for cross products of inertia. (See ref. 1 and table I.) The reference trajectories for both the longitudinal and lateral response modes are given by V, α_o, and θ_o. Equations (5) to (8) also serve to indicate the individual elements of the Y, X, U, and P vectors, as well as those of the H, D, F, and G matrices.

The remaining quantities to be determined in evaluating equation (2) are the partial derivatives $\partial \hat{Y}_i / \partial P$ generated by the matrix equations

$$\frac{\partial \hat{Y}_i}{\partial P} = H(P) \frac{\partial \hat{X}_i}{\partial P} + \frac{\partial H(P)}{\partial P} \hat{X}_i + \frac{\partial D(P)}{\partial P} U_{mi} \tag{9}$$

and

$$\frac{d}{dt}\left[\frac{\partial \hat{X}_i}{\partial P}\right] = F(P)\frac{\partial \hat{X}_i}{\partial P} + \frac{\partial F(P)}{\partial P} \hat{X}_i + \frac{\partial G(P)}{\partial P} U_{mi} \qquad \left(\hat{X}_0 = O;\ \frac{\partial \hat{X}_0}{\partial P} = O\right) \tag{10}$$

which are, respectively, obtained by differentiating equations (3) and (4). The elements of the $\partial \hat{Y}_i / \partial P$ and $\partial \hat{X}_i / \partial P$ matrices are formed according to the rule for Jacobians, whereas those for the matrices resulting from the product terms $\frac{\partial H(P)}{\partial P} \hat{X}_i$, $\frac{\partial D(P)}{\partial P} U_{mi}$, $\frac{\partial F(P)}{\partial P} \hat{X}_i$, and $\frac{\partial G(P)}{\partial P} U_{mi}$ are defined by

$$a_{ik} = \frac{\partial C}{\partial P} X = \sum_{j=1}^{N} \frac{\partial C_{ij}}{\partial P_k} x_j \tag{11}$$

Instrumentation Error Models

The instrumentation models described by the following two sets of equations define the manner in which the error sources to be analyzed are introduced in the respective simulations of the output response and the control input measurements.

Output response measurements.- The true outputs Y_i, as would be obtained in the absence of any measurement errors, are generated by evaluating equations (3) and (4) with the assumed true values of the parameters, initial states, and control inputs. Except for initial state errors, which are readily simulated by choosing $X_0 \neq \hat{X}_0$, the first group of error sources to be modeled are those associated with the indicated instrument outputs Y_{Ii}. These errors are all of a static nature and are related to Y_i by

$$Y_{Ii} = TY_i + B_i \tag{12}$$

where T is a matrix of scale factors (diagonal elements), crosscoupling, and misalinements, and B_i represents biases for each component of Y_i. For the longitudinal motions, T is defined as

9

$$T = \begin{bmatrix} \left(1 + \epsilon_\theta\right) & 0 & 0 & 0 & 0 & 0 & 0 \\ 0 & \left(1 + \epsilon_q\right) & 0 & 0 & 0 & 0 & 0 \\ 0 & -\left(\dfrac{\epsilon_{vx} + \epsilon_{xcg}}{V}\right) & \left(1 + \epsilon_\alpha\right) & 0 & 0 & -\dfrac{g}{V}\left(\dfrac{\epsilon_{vx} + \epsilon_{xcg}}{V}\right) & 0 \\ 0 & 0 & 0 & \left(1 + \epsilon_u\right) & 0 & 0 & 0 \\ 0 & 0 & 0 & 0 & \left(1 + \epsilon_{nx}\right) & -\gamma_{nx} & \left(\dfrac{\epsilon_{az} + \epsilon_{zcg}}{g}\right) \\ 0 & 0 & 0 & 0 & \gamma_{nz} & \left(1 + \epsilon_{nz}\right) & -\left(\dfrac{\epsilon_{ax} + \epsilon_{xcg}}{g}\right) \\ 0 & 0 & 0 & 0 & 0 & 0 & \left(1 + \epsilon_{\dot{q}}\right) \end{bmatrix} \quad (13)$$

where the short period approximation is obtained by deleting the fourth and fifth rows and columns (which involve Δu and Δn_x) so as to conform with the short period version of equation (5). Similarly, for the lateral-directional motions,

$$T = \begin{bmatrix} \left(1 + \epsilon_\beta\right) & 0 & -\left(\dfrac{\epsilon_{vx} + \epsilon_{xcg}}{V}\right) & 0 & 0 & 0 & 0 \\ 0 & \left(1 + \epsilon_p\right) & -\gamma_p & 0 & 0 & 0 & 0 \\ 0 & \gamma_r & \left(1 + \epsilon_r\right) & 0 & 0 & 0 & 0 \\ 0 & 0 & 0 & \left(1 + \epsilon_\phi\right) & 0 & 0 & 0 \\ 0 & 0 & 0 & 0 & \left(1 + \epsilon_{ny}\right) & -\left(\dfrac{\epsilon_{az} + \epsilon_{zcg}}{g}\right) & \left(\dfrac{\epsilon_{ax} + \epsilon_{xcg}}{g}\right) \\ 0 & 0 & 0 & 0 & 0 & \left(1 + \epsilon_{\dot{p}}\right) & -\gamma_{\dot{p}} \\ 0 & 0 & 0 & 0 & 0 & \gamma_{\dot{r}} & \left(1 + \epsilon_{\dot{r}}\right) \end{bmatrix} \quad (14)$$

The elements of T are defined in more detail in reference 1.

The next group of error sources to be simulated are those arising from the dynamic characteristics of the output measurements, which are assumed to be adequately approximated by first-order lags. The lagged outputs Y_{Li} are given by

$$\frac{d}{dt}\left(Y_{Li}\right) = \Gamma_y^{-1}\left(Y_{Ii} - Y_{Li}\right) \qquad\qquad \left(Y_L(0) = Y_I(0)\right) \quad (15)$$

10

where Γ_y is a diagonal matrix of measurement time constants. The complete output-measurements model then is obtained by adding a sequence of white noise vectors W_i to get

$$Y_{mi} = Y_{Li} + W_i \tag{16}$$

in which Y_{Li} is replaced by Y_{Ii} when lags are to be ignored, and the weighting matrix R appearing in equations (1) and (2) now is defined by

$$R\delta_{ij} = E\left[w_i w_j^T\right] \qquad \left(\delta_{ij} = \begin{cases} 1 & (i = j) \\ 0 & (i \neq j) \end{cases}\right) \tag{17}$$

where $E\left[w_i\right] = 0$ at every sample point.

Control input measurements.- The measurements of the input control surface positions U_{mi} used in evaluating equations (3) and (4) are modeled in essentially the same manner as Y_{mi}. By starting with the assumed true inputs U_i, the indicated instrument readings U_{Ii} are represented as

$$U_{Ii} = T_c U_i + B_{ci} \tag{18}$$

which is of the same form as equation (12), except that the matrix T_c is diagonal and contains only scale factor errors. As with Y_{Li} in equation (15), the dynamic characteristics of the control input measurements are also approximated by first-order lags

$$\frac{d}{dt}\left(U_{Li}\right) = \Gamma_c^{-1}\left(U_{Ii} - U_{Li}\right) \qquad \left(U_L(0) = U_I(0)\right) \tag{19}$$

where U_{Li} represents the lagged inputs and Γ_c is a diagonal matrix of measurement time constants analogous to Γ_y. The addition of a sequence of white noise vectors W_{ci} similar to W_i yields

$$U_{mi} = U_{Li} + W_{ci} \tag{20}$$

which completes the simulation of the control input measurements.

Monte Carlo Computations

The values used for the measurement errors appearing in equations (16) and (20) are listed in table I. These quantities are the zero-mean 1σ values employed in references 1 and 5 and are utilized in conjunction with a pseudo-random number generator to simulate sets of Y_{mi} and U_{mi} time histories for a number of Monte Carlo runs.

By following the simulation procedure employed in references 1 and 2, the sensor location errors $(\epsilon_{ax}, \epsilon_{az}, \epsilon_{vx})$ and the elements of Γ_y and Γ_c are treated as constants which remain fixed at their tabulated 1σ values for all sets of Y_{mi} and U_{mi} generated. The elements of W_i and W_{ci} are given new random values at each t_i of every set of Y_{mi} and U_{mi}, whereas the values for all of the remaining error sources are regenerated once for each such set so as to simulate random biases. A corresponding set of parameter estimates $\hat{P}$ are computed by means of equation (2), and the resulting estimation errors $\Delta\hat{P} = \hat{P} - P$ are formed by subtracting the assumed true parameter values. The means and variances of the $\Delta\hat{P}$ from M Monte Carlo runs then are calculated from

$$\overline{\Delta P} = E(\Delta\hat{P}) = \frac{1}{M} \sum_{j=1}^{M} \Delta\hat{P}_j \tag{21}$$

and

$$E\left(\Delta\hat{P}\Delta\hat{P}^T\right) = \frac{1}{M} \sum_{j=1}^{M} \left(\Delta\hat{P}_j - \overline{\Delta P}\right)\left(\Delta\hat{P}_j - \overline{\Delta P}\right)^T \tag{22}$$

Further computations of a similar nature are made to permit evaluating the effects of the $\Delta\hat{P}$ on the estimates of the output response trajectories and the system open-loop characteristic equation pole locations. Statistics of the former, for each value of t_i, are readily calculated from equations (21) and (22) by replacing $\Delta\hat{P}_j$ with their corresponding $\hat{Y}_i$, as generated by evaluating equations (3) and (4) with the $\hat{P}_j$. The real and complex characteristic equation roots have the respective forms

$$\left.\begin{array}{l} s = \dfrac{1}{\tau} \\[2mm] s = -\zeta\omega \pm i\omega\sqrt{1-\zeta^2} \end{array}\right\} \tag{23}$$

where the appropriate values for τ, ω, and ζ are calculated by means of the following equations from reference 6. The natural frequency ω and damping ζ for the longitudinal short period mode are given, respectively, by

$$\left.\begin{array}{l} \omega_{sp} = \sqrt{M_q Z_w - V M_w} \\[3mm] \zeta_{sp} = -\dfrac{1}{2\omega_{sp}}\left(Z_w + M_q\right) \end{array}\right\} \tag{24}$$

Similarly, for the lateral-directional motions,

$$\tau_s = \frac{L_p^*\left(Y_\beta N_r^* + N_\beta^*\right) + \frac{g}{V} L_\beta^*}{\frac{g}{V}\left(N_\beta^* L_r - L_\beta N_r\right)} \tag{25}$$

and

$$\tau_r = - \frac{N_\beta^*}{L_p^*\left(Y_\beta N_r^* + N_\beta^*\right) + \frac{g}{V} L_\beta^*} \qquad (26)$$

give the spiral divergence and roll subsidence time constants, respectively, and

$$\left.\begin{array}{l} \omega_D = \sqrt{N_\beta^*} \\[2mm] \zeta_D = - \dfrac{Y_\beta + L_p^* + N_r^* + \dfrac{1}{\tau_s} + \dfrac{1}{\tau_r}}{2\omega_D} \end{array}\right\} \qquad (27)$$

for the Dutch roll mode. As the short period roots of the longitudinal characteristic equation become real for some of the M solutions for $\Delta \hat{P}$, equations (21) and (22) are not applied to the values of $\hat{s}$; and scatter diagrams are used to indicate the distribution of these quantities.

RESULTS AND ANALYSIS

The Monte Carlo analysis of the effects of unmodeled instrumentation errors outlined in the introduction was based on simulated flight data, generated from the aircraft parameters and cruise flight conditions listed in table II and the two sets of control input maneuvers plotted in figure 1. These choices permit examining the effects of varying the information content of the simulated response measurements and the type of aircraft and facilitate comparisons with similar results presented in references 1 and 2. The effects of the unmodeled error sources were evaluated in three groups or categories, designated as error cases, which, respectively, correspond to progressively adding white measurement noise (case 0), static measurement errors (case 1), and dynamic lags and control input errors (case 2) to the simulated data. The analysis presented includes results for both the longitudinal short period and lateral-directional response modes. Lastly, sensitivity computations were performed to identify the dominant error sources.

Error Analysis

In order to extend and make possible direct comparisons with the results for the ensemble algorithm given in references 1 and 2, those for the present study also were generated mainly for a high-performance military aircraft designated herein as aircraft F (see table II) by using the input maneuvers designated as sequence 1 in figures 1(a) and 1(b). The Monte Carlo computations described previously were generally based on 50 sets

of simulated flight data; however, satisfactory statistical results were achieved in some cases with as few as 25 sets. The effects of the unmodeled instrumentation errors on the estimated aircraft parameters are analyzed; then, the corresponding perturbations to the output response trajectories and characteristic equation pole locations are discussed.

Stability and control derivatives.- The statistics of the errors in the estimated aircraft parameters, for both the short period and lateral response modes, are presented in figure 2 for each of the three error cases. This information is expressed in terms of percentage deviation from the assumed true value of each such derivative presented and includes the mean and standard deviation for every element of the resulting $\Delta \hat{P}$ as determined from equations (21) and (22). For figure 2, and for all subsequent plots of a similar nature, the mean and standard deviation of each plotted quantity are, respectively, denoted by crosshatched and solid bars as indicated.

In generating the data plotted in figure 2, the estimation errors were found to be very large for the longitudinal derivatives $\hat{M}_u$, $\hat{X}_u$, $\hat{Z}_u$, and $\hat{X}_w$, associated with the phugoid, and for the lateral derivatives $\hat{Y}_{\delta a}$ and $\hat{Y}_{\delta r}$. Further analysis indicated that these errors, which ranged up to 20 times the assumed true values of their respective derivatives for case 2, tend to be greatly exaggerated with respect to those derivatives for which the response data contain insufficient information. Since the phugoid period for aircraft F is roughly 22 times the 15-second $[t_0, t_f]$ data-sampling interval used, the results for $\hat{M}_u$, $\hat{X}_u$, $\hat{Z}_u$, and $\hat{X}_w$ were judged to be inaccurately determined because of insufficient information, and only those for the derivatives retained in the short period approximation are presented. The values for $\hat{Y}_{\delta a}$ and $\hat{Y}_{\delta r}$ were omitted for the same reason, but these two derivatives were allowed to vary in the estimation process.

Reference to figure 2 shows that the static errors added by case 1 cause much larger parameter inaccuracies than those due to white measurement noise alone (case 0) and produce biases in most of the elements of $\Delta \hat{P}$ for both response modes which are comparable to their respective standard deviations. These biases proved to be caused mainly by the constant errors ϵ_{ax}, ϵ_{az}, and ϵ_{vx} (see table I) and not by any statistical inaccuracy that could be attributed to the number of data sets used. Repeating the case 1 computations with these three error sources set to zero showed the biases to decrease by a factor of 10 or more in nearly all of the derivatives for both response modes, which essentially reduces them to a negligible level. Comparisons of the Monte Carlo results presented in figure 2 with those obtained by using the ensemble algorithm generally indicated good agreement but were limited to cases 0 and 1 since case 2 was not evaluated in references 1 and 2. With the exception of some of the weaker derivatives, the differences amounted to only a few percent in both the mean and random components of $\Delta \hat{P}$. The results for case 2 show that dynamic lags and control input errors can cause much larger inaccuracies in the estimated derivatives than the combined effects of white noise and static errors in the response measurements.

14

The effects of initial state errors were also evaluated; however, the resulting changes in $\Delta\hat{P}$ proved to be very small (about equal to those for case 0) so that the utility of estimating X_o would seem questionable for either case 1 or case 2. Since the results for case 1 imply that the contributions to $\Delta\hat{P}$ from the biases in the response measurements are small compared to those from the dynamic lags and control input errors, the value of estimating the elements of B also appears doubtful. Estimating case 2 error sources (assuming they are present in the flight data) would, therefore, seem to offer better prospects for reducing inaccuracies in the estimated derivatives. One further aspect of the computations that should be mentioned is that $\left(\dfrac{\partial\hat{Y}_i}{\partial P}\right)^T R^{-1}\left(\dfrac{\partial\hat{Y}_i}{\partial P}\right)$ remained almost unchanged for all three error cases, so that the inverse of this matrix is not indicative of the error covariance matrix $E\left[\Delta\hat{P}\Delta\hat{P}^T\right]$ except for case 0.

Output response trajectories.- The effects of $\Delta\hat{P}$ on the resulting output response trajectories are illustrated by the time-history curves presented in figure 3. Plotted for each element of the short period and lateral output vectors are the assumed true response (based on the parameter values in table II taken from refs. 7, 8, and 9) and also the means and standard deviations of both the measured and estimated response as calculated from equations (21) and (22). Only the curves for case 2 are plotted since those for cases 0 and 1 exhibit almost no deviation from the true trajectories. These results show that the perturbations to the response trajectories are not very severe; however, their importance depends on the particular application.

Reference to figure 3 indicates that the largest perturbations for both response modes occur for the attitude angles and increase to fairly large values over the 15-second interval plotted. The reason for this propagation was traced to the effects of the $\Delta\hat{P}$ on the integration of the aircraft equations of motion. Inspection of equation (6) for the short period mode shows that the errors in $\hat{M}_q$, $\hat{M}_w$, and $\hat{M}_{\delta e}$ directly affect the integration of $\Delta\hat{q}$. The resulting inaccuracy in $\Delta\hat{q}$ is, in turn, propagated by the integration of $\Delta\hat{\theta}$, so that the effect on the pitch attitude error $\Delta\hat{\theta}$ is twofold. Equation (8) for the lateral mode indicates that the roll attitude error $\Delta\hat{\phi}$ results from a similar double propagation of the errors in $\hat{L}_\beta^*$, $\hat{L}_p^*$, $\hat{L}_r^*$, $\hat{L}_{\delta a}^*$, and $\hat{L}_{\delta r}^*$ by the integration of $\Delta\hat{P}$ and $\Delta\hat{\phi}$. The perturbations to the attitude angles $\Delta\hat{\theta}$ and $\Delta\hat{\phi}$ thus depend on the errors in these eight derivatives, which all increase appreciably between cases 1 and 2. (See fig. 2.)

The relative positions of the $\hat{Y}_i$ and Y_{mi} time histories plotted in figure 3 further indicate the effects of the unmodeled instrumentation errors on the fit between the estimated and measured response curves, which appears to be generally good except for the attitude angles $\Delta\hat{\theta}$ and $\Delta\hat{\phi}$. The estimated response curves (except that for $\Delta\hat{\phi}$) exhibit negligible biases, but their standard deviations are larger than those for the

corresponding measured curves. This behavior of the standard deviation curves is opposite to that observed for cases 0 and 1 (where some compensation of the measurement errors by the algorithm is evident), and it may be due to process noise introduced in equations (3) and (4) by control input errors (case 2) which degrades parameter estimates obtained with the modified Newton-Raphson algorithm. (See ref. 10.)

Characteristic equation pole locations.- The s-plane representation is employed for the scatter diagrams presented in figure 4 to illustrate the effects of $\Delta \hat{P}$ on the resulting characteristic equation pole locations. The plotted pole locations for both response modes were calculated from equations (24) to (27) and include data points for each of the M sets of $\hat{P}$ used in generating figures 2 and 3. The results for the different poles are denoted by plotting symbols as shown, and their assumed true locations (based on the parameter values in table II) are indicated by arrows. As was the case with figure 3, only the results for case 2 are presented since those for cases 0 and 1 also showed very little departure from the true values. Although the perturbations to the characteristic equation pole locations do not appear to be much more severe than those for the response trajectories, their importance again should be judged by the application.

In addition to scatter, each group of estimated pole locations plotted in figure 4 exhibited biases which were largest for the short period and roll subsidence poles. Evaluation of equations (24), with only the mean components of the errors in $\hat{M}_q$, $\hat{M}_w$, and $\hat{Z}_w$ included, yielded a surprisingly accurate value for the bias in the estimated short period pole locations. Further computations showed that the mean error in $\hat{M}_q$ alone accounted for roughly 95 percent of the total bias. Similar evaluations of equation (26) indicated that the mean error in $\hat{L}_p^*$ dominated the bias in the estimated roll-subsidence pole location to nearly the same extent. Reference to figure 2 again showed that the errors in those derivatives which dominated the resulting perturbations increased appreciably between cases 1 and 2.

Effect of Control Input Manuever

In order to determine how the results presented in figures 2, 3, and 4 might vary for an alternate choice of control inputs, which also change the information content of the aircraft response, corresponding data were generated by using the input maneuvers designated as sequence 2 in figures 1(c) and 1(d). The sequence 2 inputs for both response modes are comprised of ordinary short doublet pulses and were chosen to provide a comparison with results for maneuvers of the type often used in actual flight tests. As evident from figure 1, these inputs differ both in form and duration from those for sequence 1 which consist of doublets augmented with trailing step pulses.

In order to facilitate comparisons of the parameter estimation errors for the two sets of input maneuvers, the ratio of $\Delta \hat{P}$ for sequence 2 to that for sequence 1,

$\Delta\hat{P}_2/\Delta\hat{P}_1$, is plotted in figure 5 for each of the short period and lateral derivatives. The actual $\Delta\hat{P}_2$ percentage values can easily be obtained by multiplying $\Delta\hat{P}_1$ by $\Delta\hat{P}_2/\Delta\hat{P}_1$ if desired. For example, the values of $\Delta\hat{P}_1$ and $\Delta\hat{P}_2/\Delta\hat{P}_1$ for the mean error in $\hat{L}_p^*$ (from figs. 2 and 5) are, respectively, about 20 percent and 0.5, which give 10 percent as the value of the mean error in $\hat{L}_p^*$ for sequence 2.

Except for the ratios of the mean errors in some of the lateral derivatives for case 0 (which are inaccurately formed because of round-off errors arising from the smallness of the numbers involved), the fact that the values for most of the $\Delta\hat{P}_2/\Delta\hat{P}_1$ ratios plotted in figure 5 are nearly unity indicates essentially the same magnitude $\Delta\hat{P}$ errors for both sets of inputs. Even though the aircraft response differs substantially, as evident from the corresponding state variable time histories also plotted in figure 1, the increase in information content afforded by the use of sequence 1 did not result in any appreciable decrease in $\Delta\hat{P}$. Thus, the information content of the response data does not appear to be deficient for either set of input maneuvers. Although the assumed true response trajectories for the two sets of inputs also exhibit the differences just noted, the magnitudes and overall characteristics of the resulting perturbations are essentially the same for each corresponding element of $\hat{Y}_i$. The two sets of characteristic equation pole locations showed even smaller differences, which is consistent with the fact that the parameter estimation accuracy remained almost unchanged. Because of the limited additional information they contribute, the response trajectories and pole location plots for sequence 2 are not presented for either response mode.

Comparisons With Results for Different Classes of Aircraft

In order to further determine how the effects of the unmodeled instrumentation errors might vary for different aircraft, the previous computations were repeated by using the parameters and nominal flight conditions for the large commercial transport aircraft designated herein as aircraft T and for the light general aviation aircraft designated herein as aircraft G also listed in table II. These data include results for both the short period and lateral response modes, and they were generated by using the sequence 1 input maneuvers. The ratio of $\Delta\hat{P}$ for aircraft T and aircraft G to that for aircraft F, that is, $\Delta\hat{P}_T/\Delta\hat{P}_F$ and $\Delta\hat{P}_G/\Delta\hat{P}_F$, was formed in the same manner as $\Delta\hat{P}_2/\Delta\hat{P}_1$ to facilitate comparisons of the results for the three types of aircraft. The values of $\Delta\hat{P}_T/\Delta\hat{P}_F$ are presented in figures 6(a) and 6(b), and those for $\Delta\hat{P}_G/\Delta\hat{P}_F$ in figures 6(c) and 6(d). Although $\Delta\hat{Z}_{\delta e}$ was estimated, no results for $\Delta\hat{Z}_{\delta e}$ are included in figure 6(c) since the assumed true value for this derivative was zero for aircraft G. (See table II.) As with figure 5 some of the case 0 ratios are inaccurate; however, these results are of minor importance as the elements of $\Delta\hat{P}$ for each of the three aircraft are all very small for case 0 anyway. The $\Delta\hat{P}_T/\Delta\hat{P}_F$ ratios plotted in figures 6(a)

and 6(b) indicate that the elements of $\Delta\hat{P}$ for aircraft T and F are about the same for the short period mode but are generally larger for most of the aircraft T lateral derivatives (particularly the case 2 values for strong derivatives such as L_β^* and N_β^* as previously discussed in conjunction with fig. 3). The corresponding values of $\Delta\hat{P}_G/\Delta\hat{P}_F$ presented in figures 6(c) and 6(d) exhibit even larger differences between the two sets of parameter estimation errors for each response mode. These results indicate that the effects of unmodeled instrumentation errors on $\hat{P}$ can vary appreciably for different classes of aircraft.

The perturbations to the output response trajectories for aircraft T and G also exhibited much the same overall characteristics as those for aircraft F; and the plots for these curves were, therefore, omitted for the same reason as those for sequence 2. The corresponding plots for characteristic equation pole location for case 2, however, are presented in figure 7. Comparisons of figures 4 and 7 indicate that the pole location errors for aircraft T and G are very similar to those for aircraft F, except those for the aircraft G short period poles which exhibit a much larger scatter pattern. Evaluations of equations (24), similar to those performed in conjunction with figure 4, showed the increased scatter to be caused mainly by $\Delta\hat{M}_w$ and $\Delta\hat{Z}_w$ which are much larger for aircraft G than for either aircraft T or F. The effects of the errors in these derivatives are further manifested by the fact that the short period roots of the longitudinal characteristic equation become real and unequal for 5 of the 50 sets of pole locations plotted in figure 7(c).

Identification of Dominant Error Sources

The remaining objective of the present study was to identify which of the error sources modeled in equations (16) and (20) dominate the resulting perturbations plotted in figures 2, 3, and 4. The initial phase of this process showed that, although $\Delta\hat{P}$ for error case 1 is much larger than that for case 0, neither white noise nor static errors in Y_{mi} proved to have much effect on either the estimated response trajectories or characteristic equation pole locations. These error sources thus appeared to be relatively unimportant, indicating that the perturbations to $\hat{Y}_i$ and $\hat{s}$ evident in figures 3 and 4 were produced mainly by the effects of the dynamic lags and control-input errors.

The addition of only dynamic lags, as given by equations (15) and (19), to case 1 was found to produce negligible changes in the random components of $\Delta\hat{P}$ for both the short period and lateral derivatives, but the magnitudes of the mean or bias components generally increased. Results generated by including the individual elements of Γ_y and Γ_c one at a time indicated that these changes are produced principally by the $\tau_{\dot{q}}$ and $\tau_{\delta e}$ lags for the short period mode and by $\tau_{\dot{p}}$ and $\tau_{\delta a}$ for the lateral mode. Further analysis showed that the biases in the pole locations evident in figure 4 are noticeably

18

affected by these lags, whereas the corresponding $\hat{Y}$ trajectories remain essentially unchanged. Except for the effects of static bias errors in the lateral control input measurements, as discussed in the following paragraph, the resultant biases in $\Delta\hat{P}$ (fig. 2) and $\hat{s}$ (fig. 4) for case 2 proved to be caused mainly by the two dominant lags for each response mode. Although the effects of dynamic lags do not appear to be very large for the cutoff frequencies represented by the time constants listed in table I, these values are near a threshold such that the biases they produce may increase rapidly if onboard filtering below these frequencies is employed.

The random components of $\Delta\hat{P}$ and $\Delta\hat{Y}_i$, and the scatter in $\hat{s}$ for case 2, thus were traced to the static control input errors. By adding these error sources to case 1 one at a time, as was done with the lags, the elevator white noise $(w_{\delta e})_i$ and the aileron bias $B_{\delta a}$ were found to be the dominant static control measurement errors for the short period and lateral modes, respectively. This procedure further indicated that the random parts of the perturbations evident in figures 2, 3, and 4 are caused mainly by these error sources. As mentioned previously, $B_{\delta a}$ also contributes to the resultant biases in $\Delta\hat{P}$, $\Delta\hat{Y}_i$, and $\hat{s}$ for the lateral mode. These biases are most noticeable in the roll attitude trajectory (fig. 3(b)) and in the root location for the roll subsidence time constant (fig. 4(b)). Although only results for aircraft F are discussed, the dominant error sources were determined to be the same for all three aircraft.

CONCLUSIONS

The results from a Monte Carlo analysis of the effects of unmodeled flight instrumentation errors on the estimation of aircraft stability and control derivatives indicate the following conclusions:

1. Aircraft derivatives estimated from flight data, obtained with existing instrumentation, may be in error by amounts which are comparable to their respective nominal values. The effects of these errors on the corresponding estimates of the output response trajectories and characteristic equation pole locations do not appear to be very severe; however, their importance depends on the particular application.

2. The perturbations to the estimated parameters, response trajectories, and pole locations contributed by dynamic lags and control input errors are much larger than those arising from white noise and static errors in the response data combined.

3. The effects of initial state errors and output measurement biases also are comparatively small; hence, the utility of estimating them would seem questionable particularly if the flight data contain dynamic lags or control input errors.

4. The effects of the unmodeled instrumentation errors can be greatly exaggerated if response data having low information content are used. The exaggeration is least for strong or dominant derivatives and is greatest for weak or ill-conditioned ones.

5. Although some exceptions may be noted, the magnitudes of the resulting parameter estimation errors for the same choice of input maneuvers can vary appreciably for different classes of aircraft with some tendency to be largest for light aircraft and smallest for heavy transports.

Langley Research Center,
National Aeronautics and Space Administration,
Hampton, Va., August 13, 1974.

REFERENCES

1. Sorensen, John A.: Analysis of Instrumentation Error Effects on the Identification Accuracy of Aircraft Parameters. NASA CR-112121, 1972.

2. Sorensen, J. A.; Tyler, J. S., Jr.; and Powell, J. David: Evaluation of Flight Instrumentation for the Identification of Stability and Control Derivatives. AIAA Paper No. 72-963, Sept. 1972.

3. Bryant, Wayne H.; and Hodge, Ward F.: Effects of Flight Instrumentation Errors on the Estimation of Aircraft Stability and Control Derivatives. Parameter Estimation Techniques and Applications in Aircraft Flight Testing, NASA TN D-7647, 1974, pp. 261-280.

4. Iliff, Kenneth W.; and Taylor, Lawrence W., Jr.: Determination of Stability Derivatives From Flight Data Using a Newton-Raphson Minimization Technique. NASA TN D-6579, 1972.

5. Hill, R. W.; Clinkenbeard, I. L.; and Bolling, N. F.: V/STOL Flight Test Instrumentation Requirements for Extraction of Aerodynamic Coefficients. AFFDL-TR-68-154, vol. I, U.S. Air Force, Dec. 1968.

6. Anon.: Fundamentals of Design of Piloted Aircraft Flight Control Systems. Vol. II. Dynamics of the Airplane. BuAer Rep. AE-61-4, Bur. Aeronaut., Feb. 1953.

7. McRuer, Duane; Ashkenas, Irving; and Graham, Dunstan: Aircraft Dynamics and Automatic Control. Tech. Rep. No. 129-1 (Contract No. NOw62-0781-c), Systems Technology Inc., Aug. 1968, pp. A-1 − A-56. (Available from DDC as AD 859 330.)

8. Bonine, W. J.; Niemann, C. R.; Sonntag, A. H.; and Weber, W. B.: Model F/RF-4B-C Aerodynamic Derivatives. Rep. 9842, McDonnell Aircraft Corp., Feb. 10, 1964. (Rev. Aug. 1, 1968.)

9. Leisher, L. L.; and Walter, H. L.: Stability Derivatives of Cessna Aircraft. Rep. No. 1356, Cessna Aircraft Co., May 22, 1957.

10. Stepner, David E.; and Mehra, Raman K.: Maximum Likelihood Identification and Optimal Input Design for Identifying Aircraft Stability and Control Derivatives. NASA CR-2200, 1973.

TABLE I.- STANDARD DEVIATIONS OF NOMINAL INSTRUMENTATION ERRORS

[Data taken from reference 1, except as noted]

Instrument	Subscript	Bias, B, and noise, W	Scale factor ϵ	Sensor location ϵ, m	c.g. location ϵ, m	Misalinement γ, deg	Time constant,[a] τ, s
Gyros							
Pitch attitude	θ	0.150°	0.005	----	----	---	0.333
Roll attitude	ϕ	.500°	.005	----	----	---	.333
Pitch rate	q	.100 deg/s	.005	----	----	---	.333
Roll rate	p	.100 deg/s	.005	----	----	0.60	.333
Yaw rate	r	.100 deg/s	.005	----	----	.60	.333
Accelerometers							
Forward	nx, ax [b]	0.005 g	0.005	0.305	----	0.60	0.100
Normal	nz, az [b]	.005 g	.005	.305	----	.60	.100
Lateral	ny, ay [b]	.0005 g	.005	0	----	---	.100
Pitch	$\dot{q}$	.100 deg/s²	.005	----	----	---	.333
Roll	$\dot{p}$	.100 deg/s²	.005	----	----	.60	.333
Yaw	$\dot{r}$	.100 deg/s²	.005	----	----	.60	.333
Airflow							
α-vane	α, vx [b]	0.100°	0.005	0.305	----	---	0.333
β-vane	β	.050°	.005	----	----	---	.333
Pitot tube	u	.305 m	.005	----	----	---	1.000
Control surface position potentiometers							
Elevator	δe	0.100°	0.005	----	----	---	0.500
Aileron	δa	.100°	.005	----	----	---	.500
Rudder	δr	.100°	.005	----	----	---	.500
Airframe center of gravity							
Forward	xcg	----------	----	----	0.152	---	----
Lateral	ycg	----------	----	----	0	---	----
Normal	zcg	----------	----	----	.152	---	----

[a] Data from reference 5.

[b] Subscript applies to sensor location only.

TABLE II.- REFERENCE TRAJECTORIES AND STABILITY AND CONTROL DERIVATIVES FOR AIRCRAFT TESTED

Quantity	Aircraft F[a]	Aircraft T[b]	Aircraft G[c]
Reference trajectory:			
V, m/s	252.2	251.2	54.5
α_0, deg	2.6	0	-0.7
θ_0, deg	2.6	0	-0.6
Altitude, m	6096.0	10 058.4	1524.0
Longitudinal:			
M_q, s^{-1}	-0.7192	-0.9240	-6.7346
M_w, 1/s-m	-0.0338	-0.0364	-0.1664
Z_w, s^{-1}	-0.7624	-0.8060	-2.0702
M_u, 1/s-m	-0.0015	-0.0026	-0.0020
Z_u, s^{-1}	-0.0617	-0.0735	-0.3844
X_u, s^{-1}	-0.0070	-0.0140	-0.0427
X_w, s^{-1}	0.0273	0.0043	0.0702
$M_{\delta e}$, $1/s^2$-rad	-16.2100	-4.5900	-24.3809
$Z_{\delta e}$, m/s^2-rad	-21.7514	-10.5461	0
Lateral:			
Y_β, s^{-1}	-0.1569	-0.0868	-0.1630
L_β^*, s^{-2}	-15.9779	-4.4103	-23.2641
N_β^*, s^{-2}	6.5630	2.1405	5.5036
L_p^*, s^{-1}	-1.6084	-1.1812	-11.5311
N_p^*, s^{-1}	-0.0997	-0.0204	-1.3632
L_r^*, s^{-1}	0.3840	0.3343	2.6918
N_r^*, s^{-1}	-0.3432	-0.2281	-1.2138
$Y_{\delta a}$, 1/s-rad	-0.0034	0	0
$L_{\delta a}^*$, $1/s^2$-rad	10.8972	2.1102	53.7865
$N_{\delta a}^*$, $1/s^2$-rad	0.7063	-0.0652	0.2103
$Y_{\delta r}$, 1/s-rad	0.0246	0.0222	0
$L_{\delta r}^*$, $1/s^2$-rad	2.5431	0.5490	0.9974
$N_{\delta r}^*$, $1/s^2$-rad	-3.9028	-1.1644	-6.1719

[a] Data from reference 8.

[b] Data from reference 7.

[c] Data from reference 9.
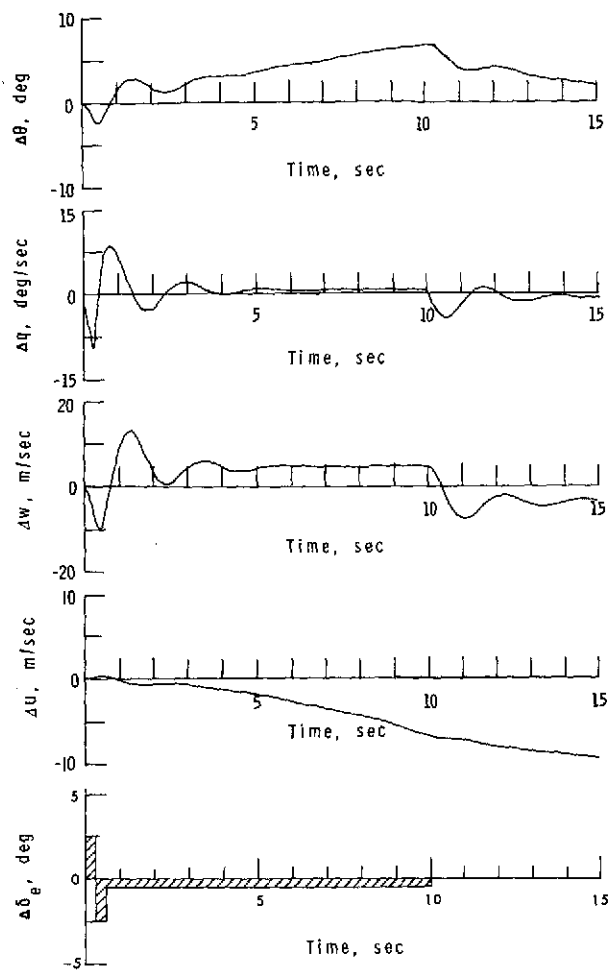
(a) Longitudinal mode.
Sequence 1.
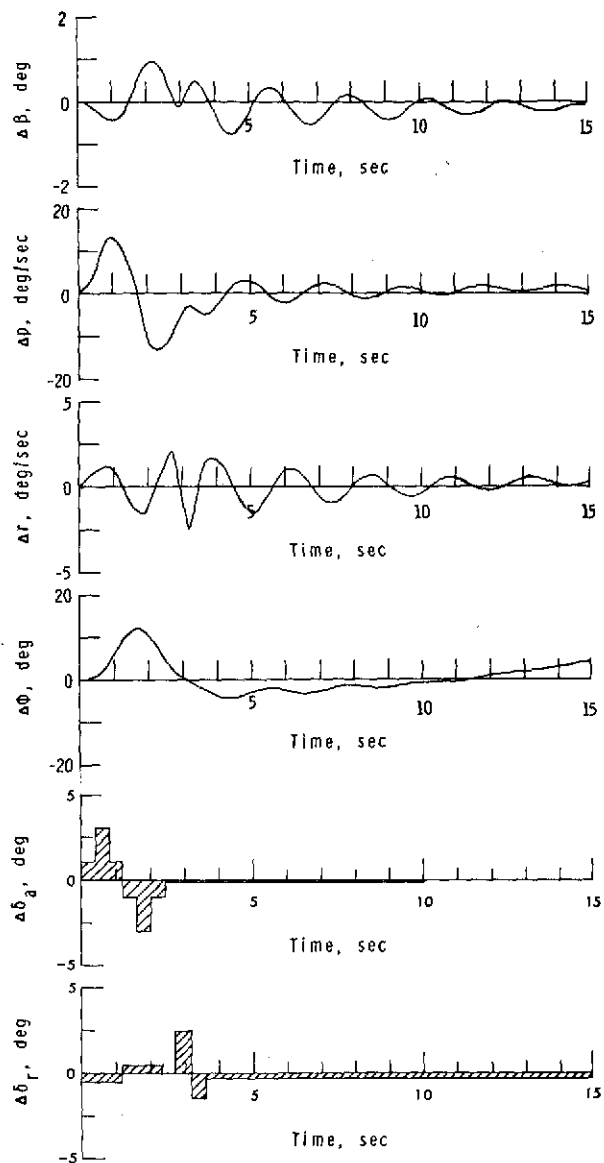
(b) Lateral-directional mode.
Sequence 1.

Figure 1.- Control input maneuvers and resulting state-
variable response trajectories for aircraft F.
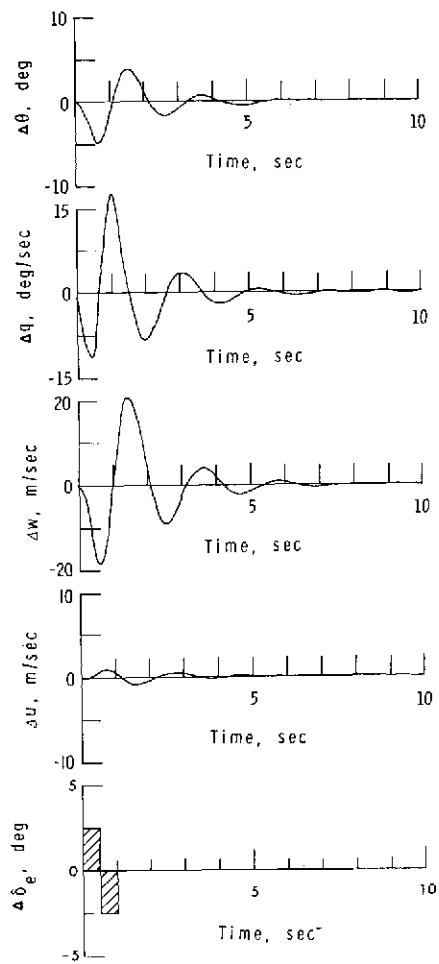
(c) Longitudinal mode.
Sequence 2.
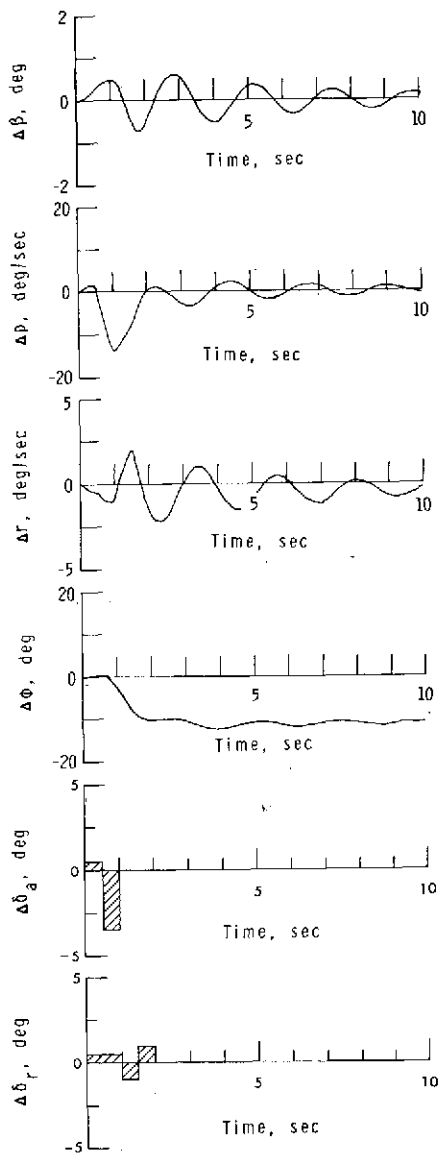
(d) Lateral-directional mode.
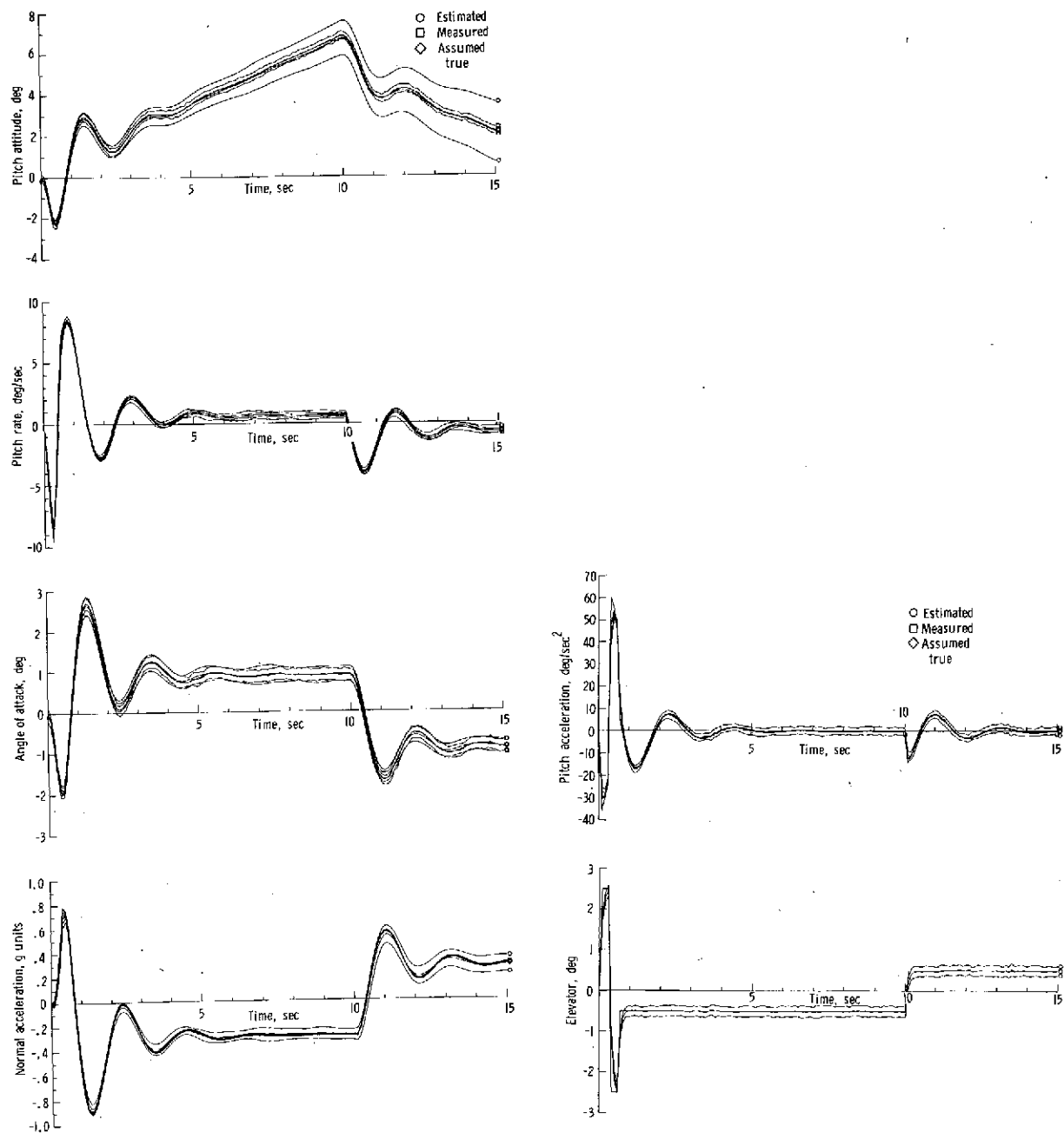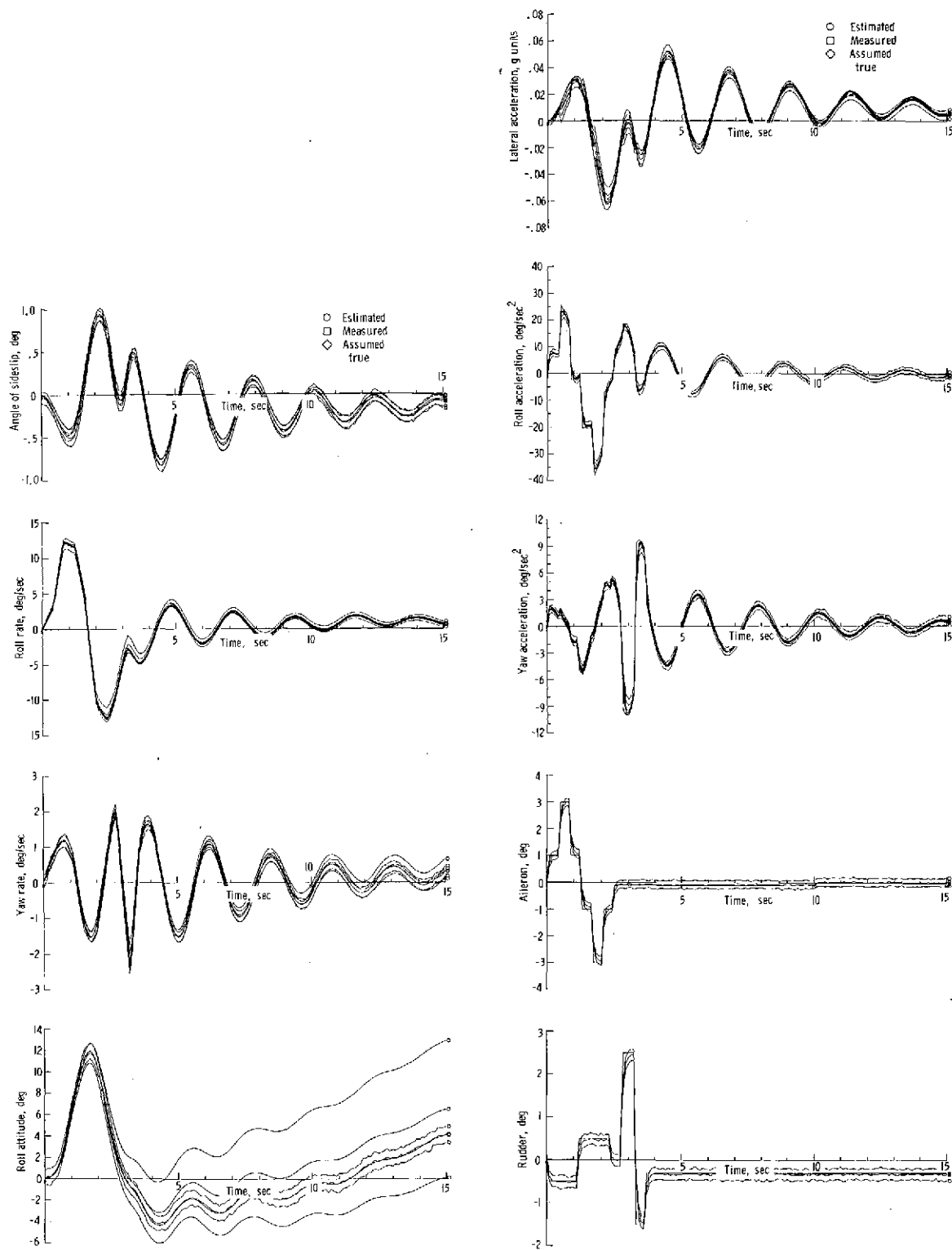Sequence 2.

Figure 1.- Concluded.
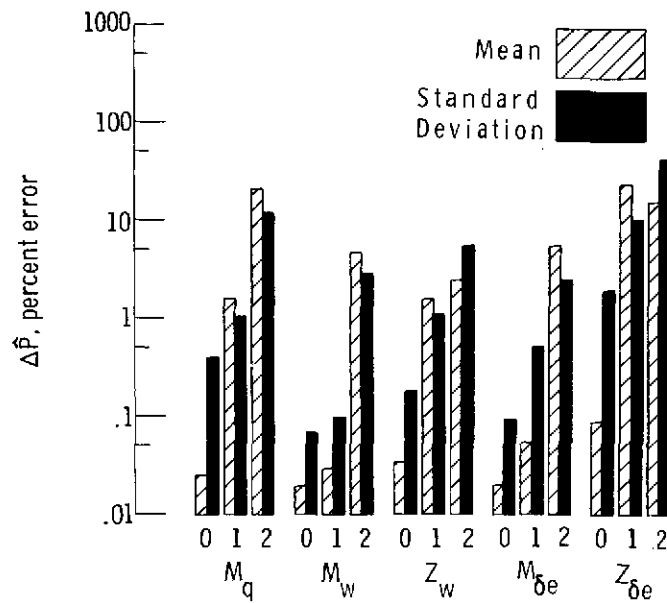
(a) Short period mode.
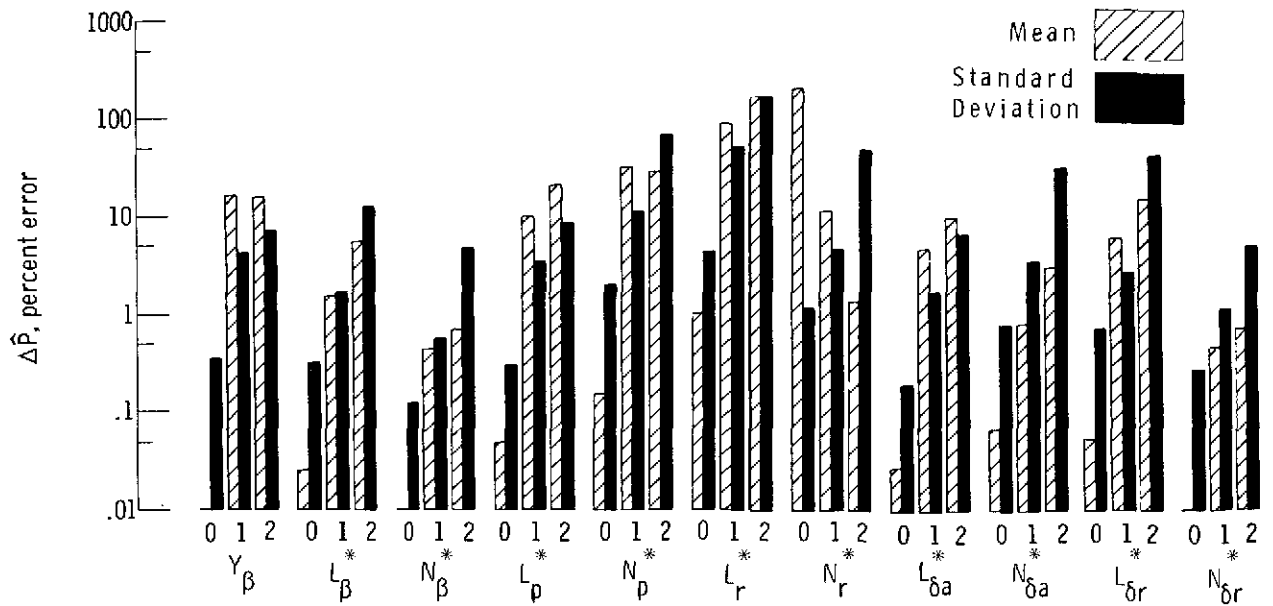
(b) Lateral-directional mode.
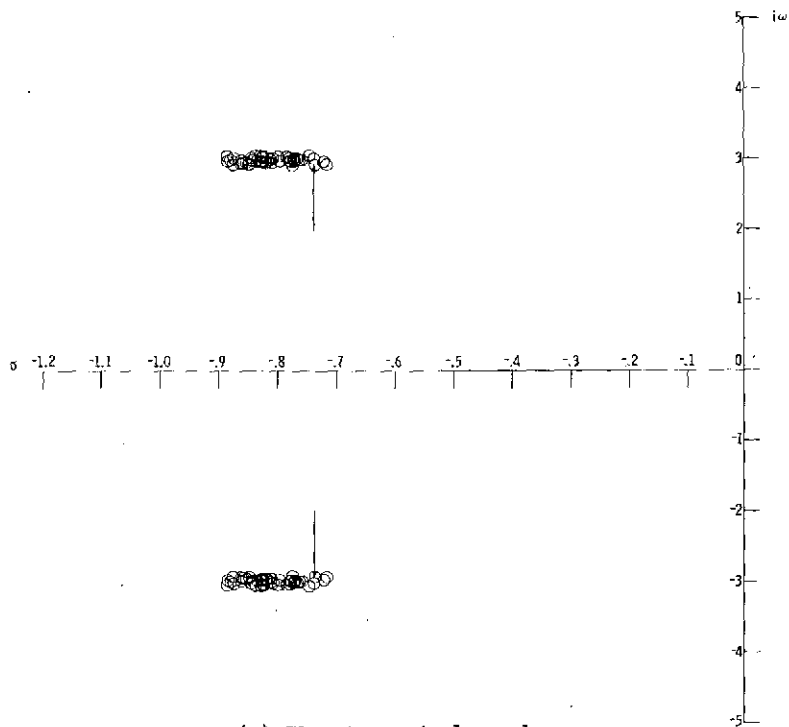
Figure 2.- Errors in estimated parameters for aircraft F.

(a) Short period measurements.
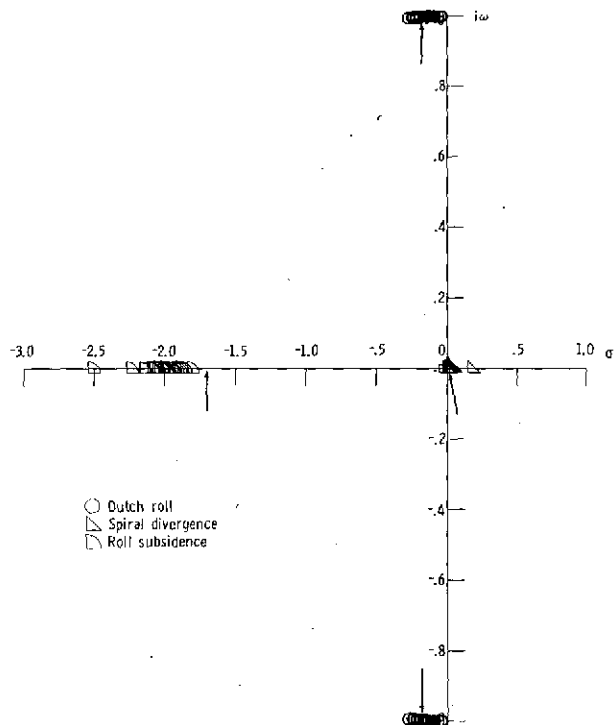
Figure 3.- Estimated, measured, and assumed true
output response trajectories for aircraft F.

(b) Lateral-directional measurements.

Figure 3.- Concluded.

(a) Short period mode.

(b) Lateral-directional mode.

Figure 4.- Estimated characteristic equation pole locations for aircraft F.
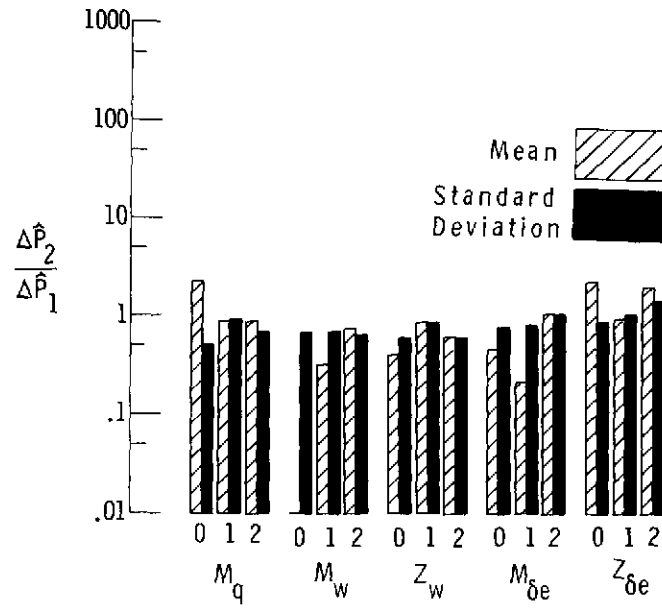
(a) Short period mode.
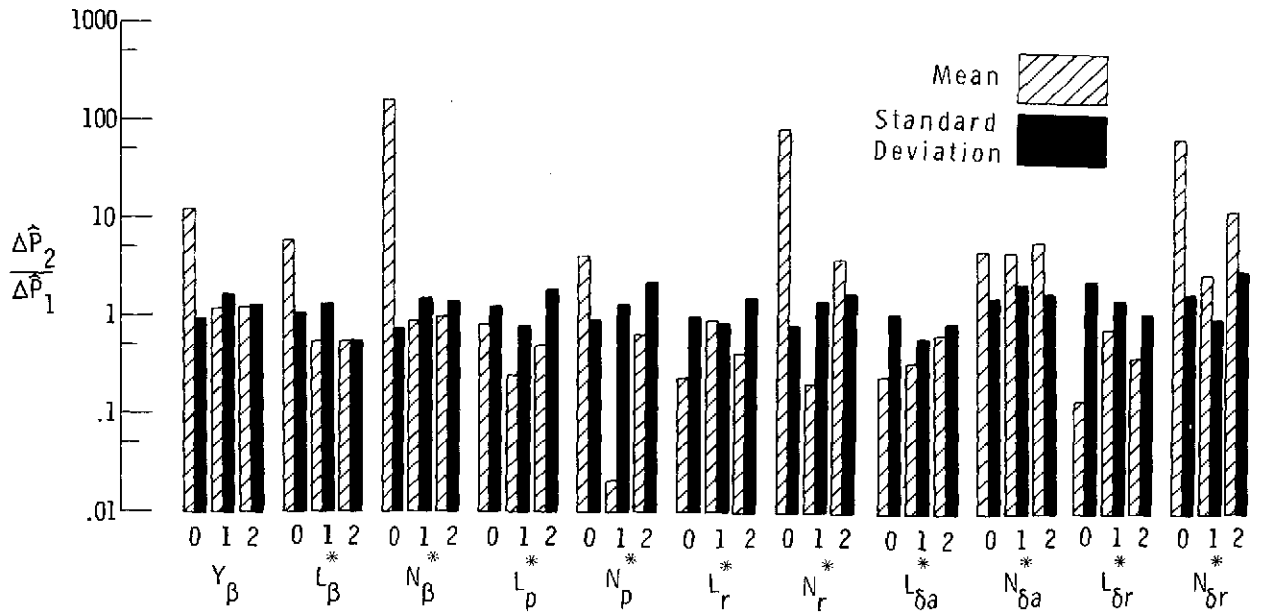
(b) Lateral-directional mode.

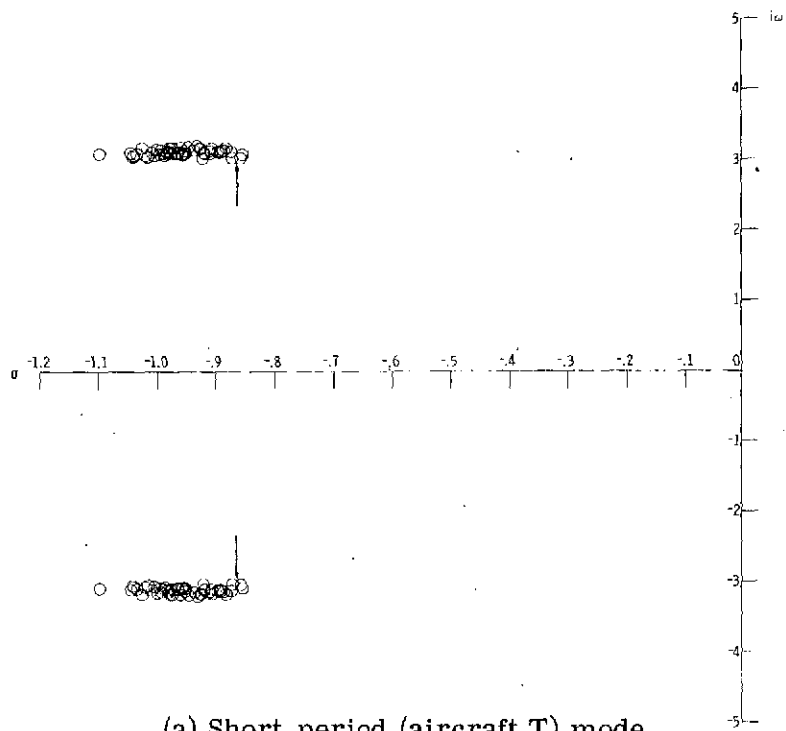Figure 5.- Effect of control input maneuver for aircraft F.
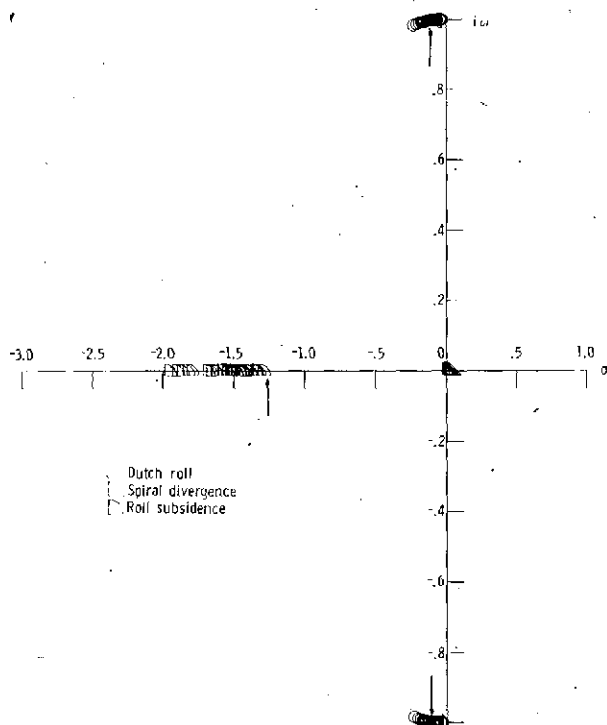
(a) Short period (aircraft T) mode.

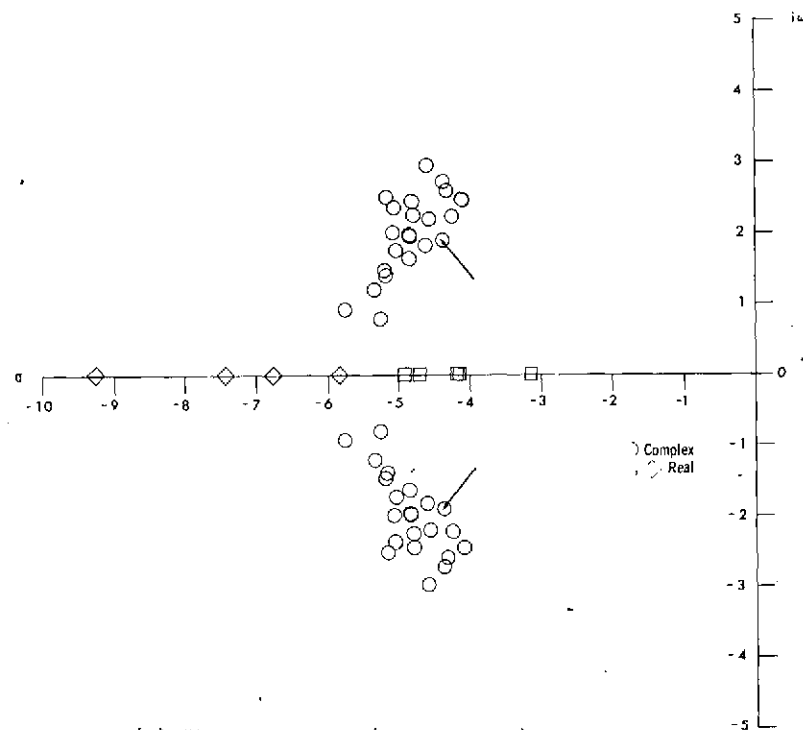

(b) Lateral-directional (aircraft T) mode.

Figure 6.- Comparison of parameter estimation errors for
aircraft T and aircraft G with those for aircraft F.
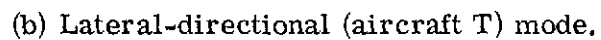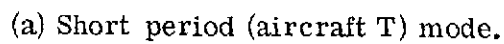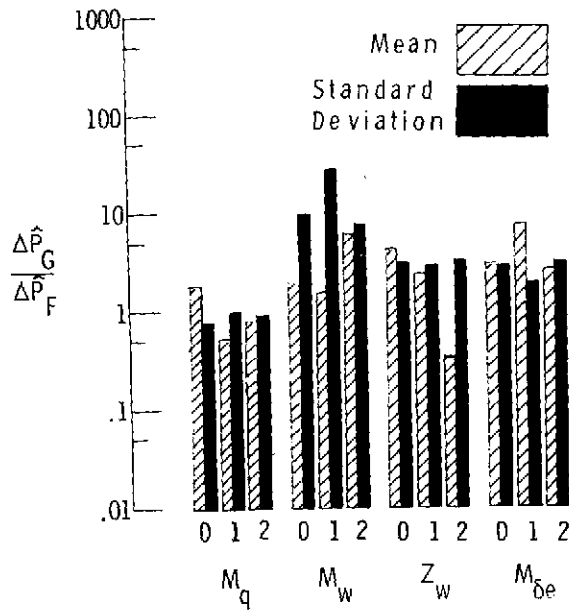
(c) Short period (aircraft G) mode.
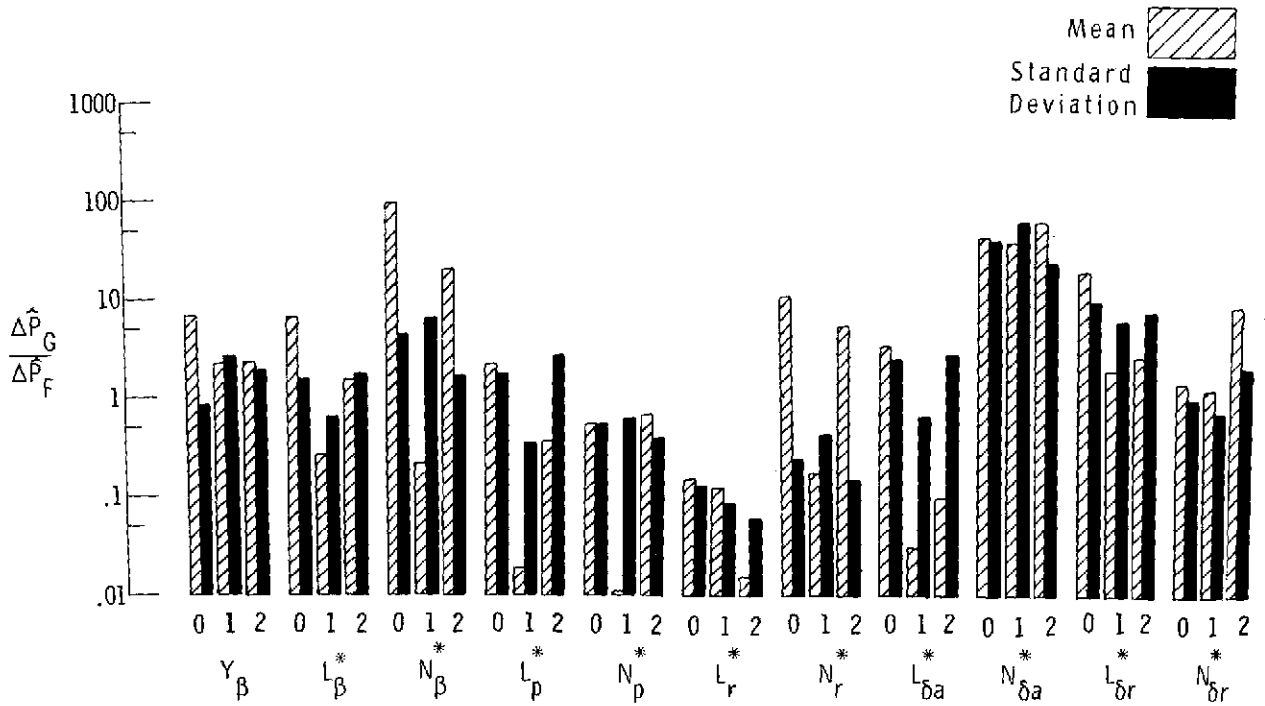
(d) Lateral-directional (aircraft G) mode.

Figure 6.- Concluded.

(a) Short period (aircraft T) mode.

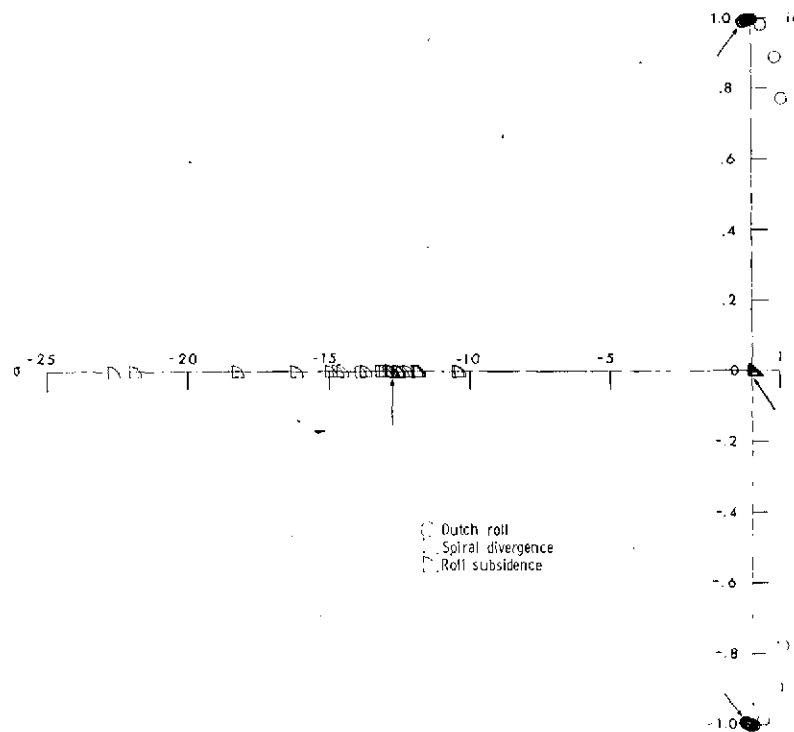Dutch roll
Spiral divergence
Roll subsidence

(b) Lateral-directional (aircraft T) mode.

Figure 7.- Estimated characteristic equation pole
locations for aircraft T and aircraft G.

(c) Short period (aircraft G) mode.

(d) Lateral-directional (aircraft G) mode.

Figure 7.- Concluded.